1-1-2021

Long-lived isomeric states and quasiparticle band structures in neutron-rich Gd 162,164 nuclei from β decay

E. H. Wang
Vanderbilt University

J. M. Eldridge
Vanderbilt University

N. T. Brewer
ORNL Physics Division

J. H. Hamilton
Vanderbilt University

J. C. Batchelder
University of California, Berkeley

See next page for additional authors

Long-lived isomeric states and quasiparticle band structures in neutron rich ^{162,164}Gd from β-decay study

E. H. Wang,[1] J. M. Eldridge,[1] N. T. Brewer,[2] J. H. Hamilton,[1] J. C. Batchelder,[3] Y. X. Liu,[4] Y. Sun,[5] C. Brown,[1] C. J. Zachary,[1] B. M. Musangu,[1] A. V. Ramayya,[1] K. P. Rykaczewski,[2] C. J. Gross,[2] R. Grzywacz,[2,6] M. Madurga,[6] D. Miller,[6] D. W. Stracener,[2] C. Jost,[6] E. F. Zganjar,[7] J. A. Winger,[8] M. Karny,[9] S. V. Paulauskas,[6] S. H. Liu,[2] M. Wolińska-Cichocka,[2,10] S. W. Padgett,[6] A. J. Mendez II,[11] K. Miernik,[2,9] A. Fijałkowska,[9] and S. V. Ilyushkin[8]

[1]*Department of Physics and Astronomy, Vanderbilt University, Nashville, TN 37235, USA*
[2]*Physics Division, Oak Ridge National Laboratory, Oak Ridge, TN 37830, USA*
[3]*Nuclear Engineering Department, University of California Berkeley, CA 94720, USA*
[4]*Department of Physics, Huzhou University, Huzhou 313000, People's Republic of China*
[5]*School of Physics and Astronomy, Shanghai Jiao Tong University, Shanghai 200240, People's Republic of China*
[6]*Department of Physics and Astronomy, University of Tennessee, Knoxville, TN 37996, USA*
[7]*Department of Physics and Astronomy, Louisiana State University, Baton Rouge, Louisiana 70803, USA*
[8]*Department of Physics and Astronomy, Mississippi State University, Mississippi 39762, USA*
[9]*Faculty of Physics, University of Warsaw, Warsaw PL-02-093, Poland*
[10]*Heavy Ion Laboratory, University of Warsaw, Warsaw PL 02-093, Poland*
[11]*Campbell University, Buies Creek, North Carolina 27506, USA*

(Dated: November 14, 2020)

Neutron-rich nuclei ^{162,164}Eu were produced by bombarding a proton beam on a ^{238}U target at the Holifield Radioactive Ion Beam Facility at Oak Ridge National Laboratory and mass seperating the ^{162,164}Eu products. New level schemes and new γ ray transitions of the daughters ^{162,164}Gd were identified from β-decay spectroscopy studies. Halflives of the ^{162,164}Eu were remeasured to clarify the previous ambiguous results. Two quasiparticle band structures were built and compared with neighboring nuclei. The β and γ bands were extended in ^{162}Gd and a γ band was extended in ^{164}Gd. Halflives of the isomeric states at (6^-) 1449 keV in ^{162}Gd and (4^-) 1096 keV in ^{164}Gd were measured to be 99(3) μs and 0.56(3) μs, respectively. Projected shell model calculations were performed and found to be in good agreement with all of the experimental data.

I. INTRODUCTION

Neutron-rich nuclei in the $A \sim 160$ region have drawn much attention in nuclear physics studies. In this region, nuclei with neutron number $N \geq 94$ become strongly deformed with large quadrupole deformations. Maximum abundance in the r-process is seen in this rare-earth region [1], and arises from this large deformation at midshell [2]. Nuclear structure studies in this region are important to understand the competion between neutron capture and β-decay in r-process stellar nucleosynthesis. From experiment, limited stucture information was known compared to other regions due to difficulties to populate the neutron-rich isotopes. Previous experimental studies show energies of the 2^+ levels have a local minimum at N=98 [3, 4]. This fact is in contrast with the theoretical calculations for deformation maximum at N=104 midshell [5]. Recently, two quasi-particle bands and isomers have been reported in ^{154,156,158,160}Nd [6, 7], ^{156,158,160,162,164}Sm [6, 8–12], ^{162,164,166}Gd [9, 12–14] by ^{238}U, ^{239}Pu induced fission and ^{252}Cf spontaneous fission.

Specifically, in the previous study of ^{162,164}Gd, ^{162}Gd excited levels up to $\sim$2.5MeV were reported in the ^{160}Gd(t,p)^{162}Gd reaction [15], with several positive parity levels assigned. Later, our group extended the ground state band up to 16^+ [3]. Recently, β-decay experiments observed a 6^- state and the 5^+, 6^+ member of the 1γ-vibrational band of this nucleus [13]. For ^{164}Gd, our previous work established the ground state band up to 14^+ [3]. Osa *et. al.* [16] observed three γ rays but did not place them in the level scheme. Additionally, several new works [9, 11, 14] based on isomeric decay from a 4^- state added two new non-yrast levels and three new γ rays to the level scheme of ^{164}Gd. In the present work, we have confirmed and extended the previous reported 1γ-vibrantional band levels and extended the band structure built on the isomeric states in ^{162,164}Gd. New spin and parity assignments have been made for the Eu parents according to our present work. Projected shell model calculations have been performed and compare favorably with the experimental data.

II. EXPERIMENTAL SETUP

The current experiment was performed at the Holifield Radioactive Ion Beam Facility (HRIBF) at Oak Ridge Naitonal Laboratory. A 10-18 μA $\sim$50 MeV proton beam was used to bombard the UCx target on a High-Voltage (HV) platform. The induced fission fragments as positive ions at 40 keV were seleted by passing through a dipole magnet with resolution of $m/\Delta m \sim 1000$. These ions were then accelerated to 200 keV and Eu was separated by a second magnet with $m/\Delta m \sim 10000$ resolution. A fast beam deflector (kicker) was used to prevent the beam from reaching the detection station. This kicker was operated in a correlated way with a tape cycle, as discussed below. The ion beam was implanted into a

TABLE I. Table of the known halflives and tape cycle time used for MTC at LeRIBSS.

Mass Number	Eu Halflife	Gd Halflife	Beam on/off
162	10.6(10) s [17]	8.2(3) min [18], 8.55(28) min [19]	22 s / 22 s
164	4.2(2) s [16]	45(3) s [20]	8 s / 8 s

movable tape at the turning point of the moving tape collector (MTC) inside the Low-energy Radioactive Ion Beam Spectroscopy Station (LeRIBSS). This point was surrounded by four high-purity germanium (HPGe) detectors and two plastic scintillators in a co-axial arragement for β detection. In the beam accumulation period, the kicker was turned on and the ion beam was transmitted to the MTC. In the decay period, the kicker was turned off to deflect the beam away. After the decay period, the MTC moved ∼50 cm away within about 400ms to a shielded place. The beam on/off settings of the tape cycle are listed in Table. I. The β detectors provided β-gated events. The acquisition system was operated in a triggerless mode and was time stamped with a 10 ns pulse from a clock. This acquisition allows for variable coincidence gates. Details of the experimental setup can be found in Ref. [21, 22]. Here A=81, 82 nuclei are the major contaminants (not from fission of Eu) because their atomic numbers are half of those the current ^{162,164}Eu ones and have similar m/Q and were selected by the magnet. The ^{162,164}Eu were in the 2^+ charge state while the contaminant A=81,82 in the beam were at 1^+, so both of them are selected by the magnet. The β-decay and β-n decay daughters of the A=81, 82 nuclei are also present but weaker.

III. EXPERIMENTAL RESULTS

A. ^{162}Gd

The new level scheme of ^{162}Gd is shown in Fig. 1. The γ ray transition intensities are measured and listed in Table. II. The energy levels are grouped into 6 bands. The ground state band was established up to 16^+ in Ref. [3] from ^{252}Cf spontaneous fission. In the present work, the g.s. band is confirmed up to 8^+. In Ref. [15], 864- keV 2^+, 930- keV 3^+ and 1015- keV 4^+ were assigned as the γ-vibrational band levels without linking transitions and were reported to have about 7 keV uncertainty. In the present study, these levels are confirmed more accurately as 863.0, 927.4 and 1012.7 keV, respectively, by identifying the linking transitions from the γ-vibrational band to the g.s. band. The 630-, 755-, 884-, 1010- keV transitions from the γ-vibrational band to the g.s. band were reported previously from the ^{162}Eu β-decay [13]. In the present work, they are identified as 628.4-, 753.7-, 881.9- and 1007.1- keV, respectively. The current work also identified the 7^+ state of the γ-vibrational band as shown in the level scheme in Fig. 1. In Ref. [23], the 863.3- and 792.0- keV transitions depopulating the 863.3- keV 2^+ γ band level, as well as the strong 856.5- keV transition depopulating the 927.9- keV 3^+ γ band level were reported. Those transitions and levels are confirmed in the present work. The odd and even spin levels of the γ band are seperated to make them easy to be seen in the figure since their energies are too close. The 12 levels located on the left of the level scheme are assumed as non-band levels. The decay patterns of those levels indicate different spin ranges. The 2305, 2414, 2418 and 3573 keV

TABLE II. The relative intensities (I_γ) of the γ ray transitions in ^{162}Gd from the current experiment. The γ ray intensities are normalized to the 164.8 keV transition. Tentative transitions are listed with parenthesis. The error bar is about 0.2 keV at 0 keV, 0.5 keV below 1MeV, and 1 keV for transition energies above 1MeV.

E_i (keV)	E_γ (keV)	I_γ (%)	E_f (keV)	E_i (keV)	E_γ (keV)	I_γ (%)	E_f (keV)
71.7	71.7	29(3)	0	1581.7	133.1	5.4(7)	1448.6
236.5	164.8	100(5)	71.7	1645.3	152.2	0.1(1)	1493.1
490.1	253.6	51(3)	236.5		1408.8	<0.6	236.5
826.0	335.9	10(1)	490.1	1701	838	1.5(5)	863.0
863.0	791.4	27(3)	71.7	1714.8	133.1	0.4(1)	1581.7
	862.9	22(1)	0	1720.8	141.6	1.7(6)	1579.3
927.4	(64.4)	<1	863.0		264.5	1.1(3)	1457.1
	691.4	5.2(4)	236.5	1733.8	152.1	1.3(2)	1581.7
	855.7	29(3)	71.7		284.0	0.8(2)	1448.6
1012.7	776.5	7.1(6)	236.5	1781	918	2.8(8)	863.0
	940.7	0.9(3)	71.7	1898.0	252.7	<0.6	1645.3
1118.4	191.4	1.0(2)	927.4		1407.9	<0.6	490.1
	628.4	9.3(7)	490.1		(1661.5)	<0.5	236.5
	881.9	44(2)	236.5	1975.4	526.8	9.7(5)	1448.6
1243.7	125	<0.5	1118.4	2015	1778	1.5(4)	236.5
	230.7	0.8(1)	1012.7	2030	1794	1.8(5)	236.5
	753.7	10(1)	490.1	(2148)	(2148)[a]	<3	0
	1007.1	7.5(6)	236.5	2305	2233	5.7(19)	71.7
1354.2	341.9	1.4(2)	1012.7	(2322)	(874)[a]	<2	1448.6
	426.5	5.4(3)	927.4	2337.2	755.5	1.4(4)	1581.7
	491.0	13(2)	863.0	2414	2342	2.5(12)	71.7
1388.0	270.0	0.7(2)	1118.4	2418	2346	3.0(13)	71.7
	898.2	3.5(4)	490.1	2590	2354	1.2(4)	236.5
1427.8	1356.1	5.1(12)	71.7	2655	2165	1.6(5)	490.1
1448.6[b]	205.2	8.9(5)	1243.7	3424	3187	2.6(7)	236.5
	329.9	42(2)	1118.4	3510	3274	0.7(3)	236.5
1457.1	102.7	2.6(6)	1354.2	3573	3501	4.9(20)	71.7
	443.4	0.9(2)	1012.7	3596	2770	1.4(4)	826.0
	529.8	2.0(4)	927.4		3106	3.4(9)	490.1
1493.1	1256.6	4.8(5)	236.5	3660	(1339)[a]	<1	(2322)
1519.7	71.1	1.2(2)	1448.6		3170	2.1(6)	490.1
1579.3	122.2	2.2(7)	1457.1		3424	1.0(4)	236.5

a: not placed in the level scheme in Fig. 1.

b: $t_{1/2}$=99(3) μs isomer. See Fig. 5.

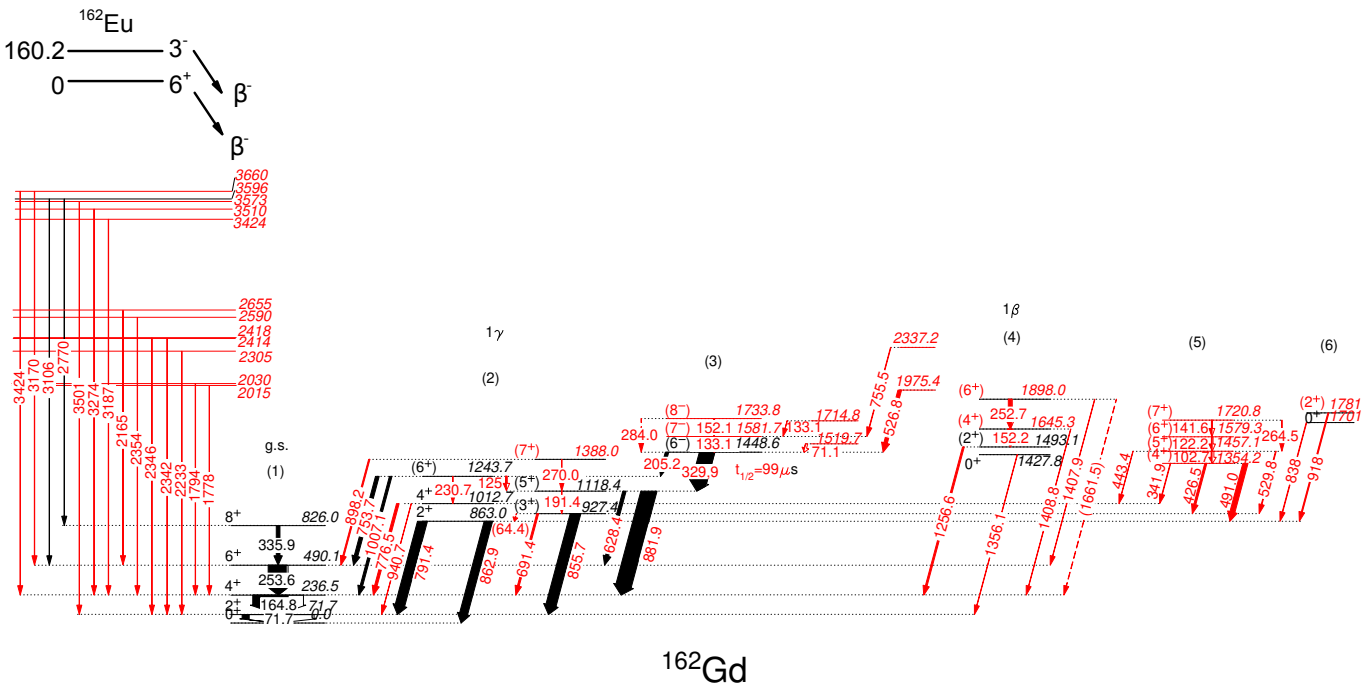

FIG. 1. (Color online)The new level scheme of ^{162}Gd obtained in the present work. New transitions and levels are labeled in red.

levels only decay to the 71.7- keV 2^+ state. They are proposed to have a lower spin (1,2,3). The 2015-, 2030-, 2590-, 3424- and 3510- keV levels only decay to the 236.5-keV 4^+ state. Those levels could have intermediate spins. The 2655-, 3596- and 3660- keV levels are likely to have relatively high spins according to their decay patterns.

Fig. 2 shows a γ ray total spectrum from about 0 to 5 MeV. All the strong γ rays from ^{162}Gd as well as contaminations are labeled. The major contaminations of this experiment are from the decays of the mass 81 decay chain. The ^{126}Te contaminations are from the last experiment in this facility. Unknown contamination transitions from the residue of the past experiment and Fe are also labeled. A prompt-prompt γ-γ ray matrix was built within a 1 μs time window, which is the time response of the prompt γ rays for the current Clover detectors. Fig. 3 depicts a γ ray coincidence spectrum by gating on the 164.8- keV transition in the g.s. band showing evidence for the new and previously reported transtions. In this gated spectrum, one can clearly see the 72, 205, 254, 330, 336, 427, 443, 628, 691, 754, 776, 882, 898, 1007 and 1257 keV transitions. Fig. 4 denotes a gate on the 491- keV γ ray. The 103, 122, 142 and 264- keV transitions in band (5) and the 791 and 863 keV transitions linking band (2) to band (1) can be seen. In the data analysis with the prompt-prompt γ-γ ray matrix, most of the strong contaminations and scatter contaminations (labeled as "C" and "S" in Fig. 3) can be identified by simply doing background subtraction. In some complicated cases, e.g. transition energies are close to each other, those contaminations as well as real peaks can be identified by gradually changing the gated energy around the aiming gated energy and comparing the behavior of peaks in such a list of gated spectra. A strong contamination will keep the position and intensity as gated energy changes. A scatter contamination will keep the intensity but change the position of the peak in an opposite direction as gated energy changes. The strong contaminations and scatter contaminations are also discussed in the ^{164}Gd part.

In Ref. [13], a 1453 keV (6^-) state was reported without a lifetime measurement. This state is confirmed at 1449- keV as an isomer in the current work. The 205 and 330- keV transitions depopulating the 1449- keV level are strong in Fig. 2 but are almost not seen in the β-gated 1 μs prompt γ ray spectrum. By summing the 205 and 330 keV transitions gated β to γ time decay curve (up to 1ms), a constant plus exponential decay is used to fit the halflife of the 1449 keV isomer. In the current work, the measured halflife of this isomer is 99(3) μs, as shown in Fig. 5.

Since the halflife of the 1449 keV level is measured, a proper β-gated prompt-delayed γ-γ matrix has been built to identify the transitions feeding this isomer. In the matrix, the prompt γ ray transition is defined from 0-1 μs after a β event, while the delayed γ ray is defined from 1-500 μs after the β event. The spectra of two gates on the delayed 330- keV γ ray and delayed 205- keV γ ray are shown in Fig. 6. In these two gates, one can see the strong 133 and 527 keV transitions as well as the weak 71, 152, 284 and 755 keV transitions. The placement of these transitions in the level scheme in Fig. 1 is based on their

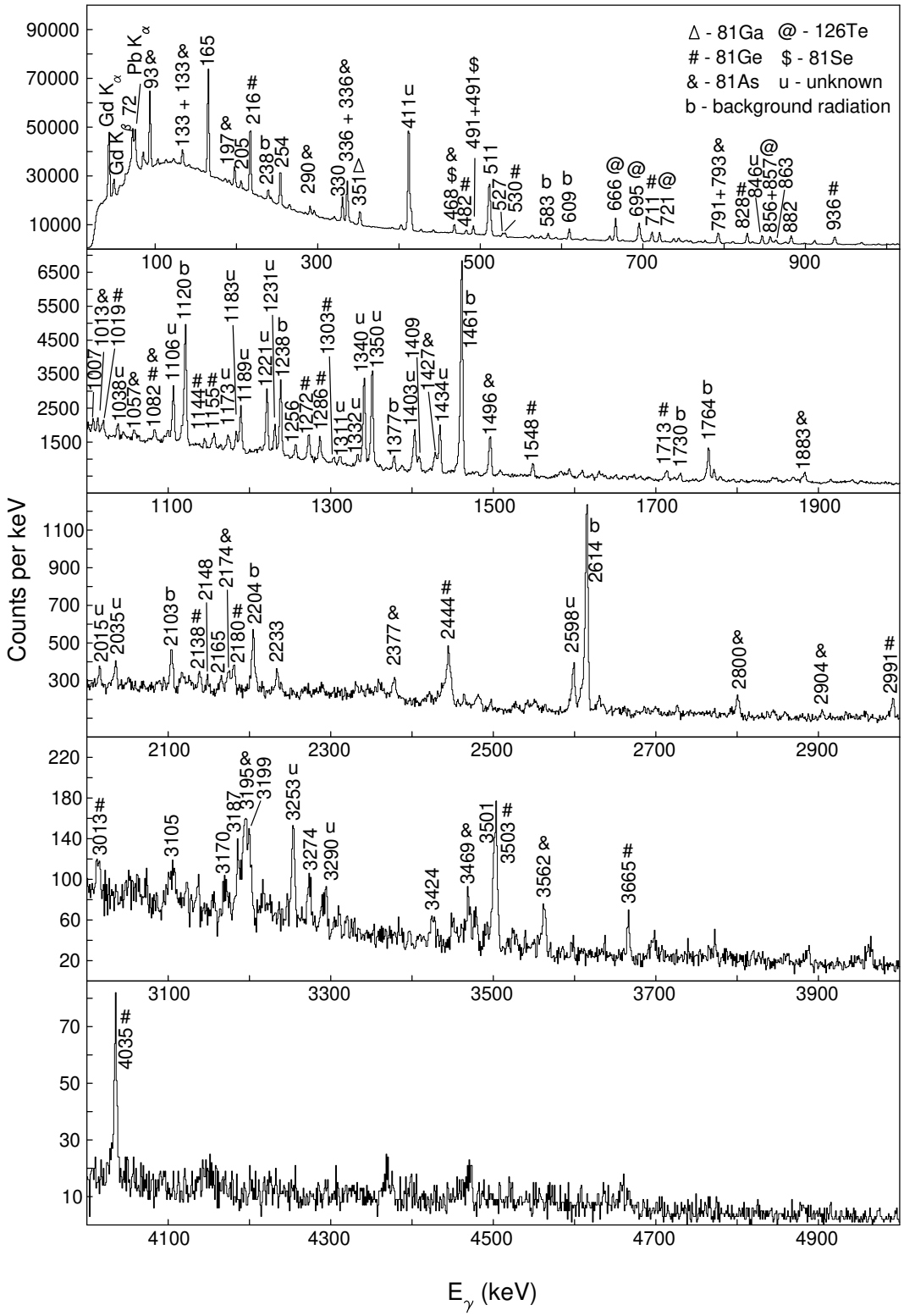

FIG. 2. The γ ray total spectrum in ^{162}Gd. Here unknown contamination γ rays labeled with "u" are weak or not in coincidence with a β ray. They are possibly from Fe isotopes. Some of the small peaks in the spectrum are weak and not in coincidence with known γ rays. The origin of those peaks are not clear and thus not labeled in the spectrum.

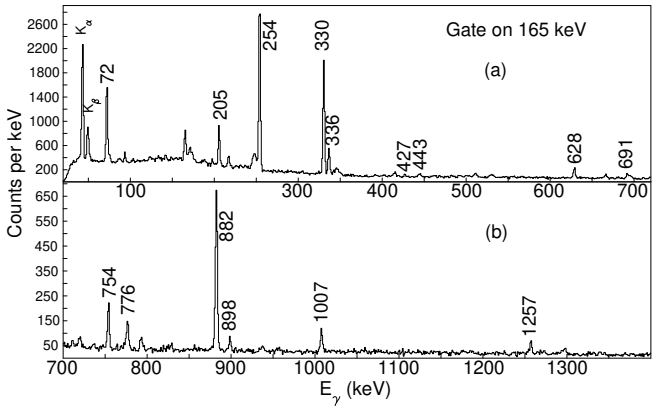

FIG. 3. Partial γ ray coincidence spectrum by gating on the 164.8 keV transition in ^{162}Gd in the prompt γ-γ matrix.

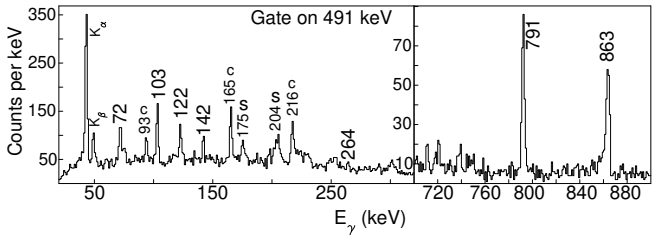

FIG. 4. Partial γ ray coincidence spectrum by gating on the 491.0- keV transition in ^{162}Gd in the prompt γ-γ matrix. In the spectrum, "c" stands for a contamination transition which is strong and in coincidence with any gated energy in this region. The "s" stands for a scattering contamination when a γ ray scatters from one detector to another. For a scattering contamination, the sum of gated energy and the scattering energy is equal to a strong transition energy.

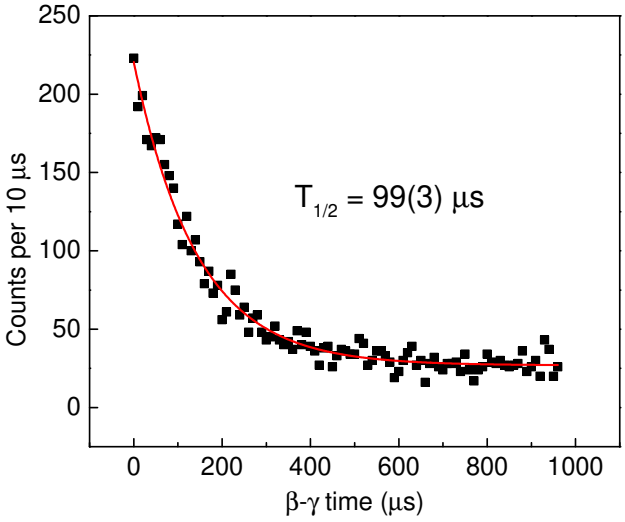

FIG. 5. (Color online) Halflife measurement of the (6$^-$) 1449 keV level. The x axis is the time difference between the β and the 205, 330 keV transitions.

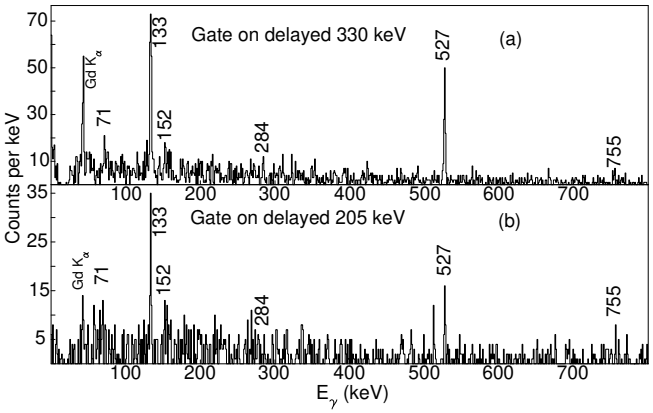

FIG. 6. Partial background subtracted γ ray coincidence spectra (a) by gating on the 329.9 keV delayed transition, and (b) by gating on the 205.2 keV delayed transition in ^{162}Gd in the β-prompt-delayed asymmetric γ-γ matrix. In this matrix, the prompt γ ray transition is defined from 0-1 μs after a β event, while the delayed γ ray is defined from 1-500 μs after the same β event.

intensities in Fig. 6 and their coincidence relationship in the prompt γ-γ matrix.

Despite the weak transitions listed as tentative in Table II, some other transitions have ambiguous assignments and may belong to either mass=79, 80, 81 or 162 nuclei. The 874 keV and 1339 keV transitions are in coincidence with each other. They are only seen in the 330 keV delayed γ gate, but not in the 205 keV delayed γ gate. Therefore, they are listed as tentative in Table II. The 2149 keV transition is not in coincidence with any γ ray in the current data. Close energy transitions at 2150 keV were reported in ^{81}Se in a ^{80}Se(n,γ) reaction [24]. This transition in ^{81}Se is not considered as the contamintation because the coincidence transitions and transitions depopulating the same levels are not seen in the current work. The 3199 keV transition in Fig. 2 is in coincidence with 43 keV and 70 keV. The coincidence 70 keV energy is 2 keV away from the 72 keV γ ray in ^{162}Gd. The 3199 keV transition was also reported in ^{80}Se [25]. Although this transition is not reported in β-decay, it may weaken its evidence in ^{162}Gd. Thus, this transition is not placed in the level scheme in Fig. 1 nor in Table II.

The parent ^{162}Eu nucleus was reported to have a 160.2(24)- keV isomer from a direct mass measurement in Ref. [13]. The ground state and the isomer of ^{162}Eu were assigned as 1^+ $\pi5/2[413]\otimes\nu7/2[633]$ and 6^+ $\pi5/2[413]\otimes\nu7/2[633]$, respectively [13]. The reported halflives of ^{162}Eu were 10.6(10) s from Ref. [16], 11.8(14) s from Ref. [26] and 15.0(5) s Ref. [13]. To explain this difference, the author in Ref. [13] assumed different halflives from the ground state and the isomer of ^{162}Eu populating low and high spins in ^{162}Gd, respectively. In the current work, different strong γ ray gates were used to measure possible different halflives. Note the ^{162}Sm nucleus halflife was reported as 2.4(5) s from the β-decay study

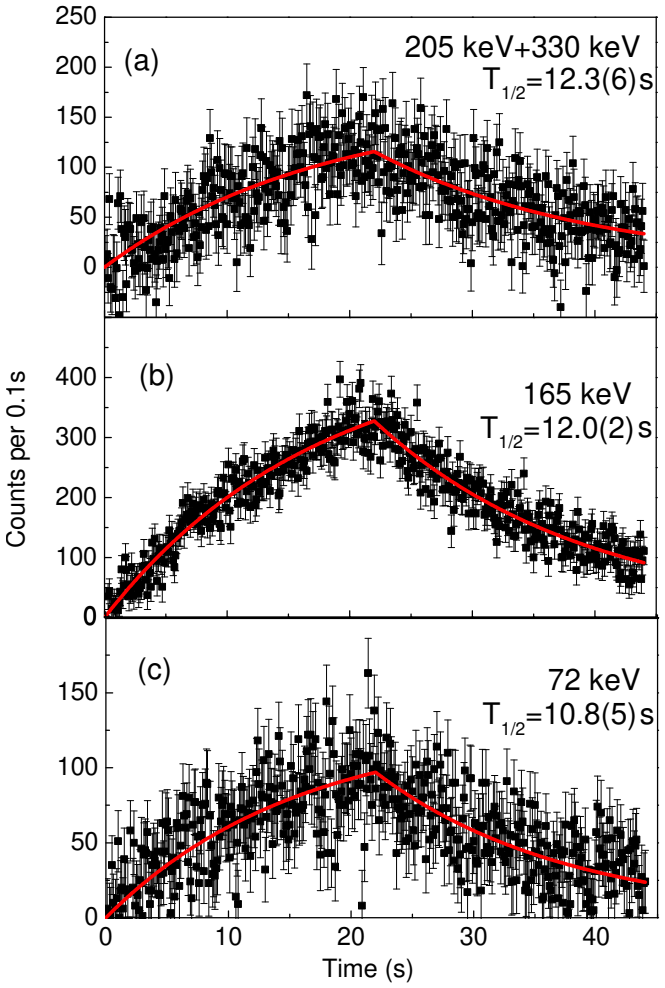

FIG. 7. (Color online) Growth and decay fitting for ^{162}Eu halflife from background subtracted (a) 205 keV and 330 keV gate, (b) 165 kV gate and (c) 72 keV gate. Note that the 72 keV gate is contaminated by the Pb x-ray.

in Ref. [27] with 36.0, 736.7 and 741.1 keV transitions assigned to the daughter ^{162}Eu nucleus. The current data do not show evidence for these three transitions neither in the γ ray total in Fig. 2, nor in the β-gated γ ray spectra. Thus, the halflife measurements in the current work do not have influence from ^{162}Sm. The halflives were fitted to grow-decay curve using the same equation as in Ref. [22] Eq. (1).

$$I_0(t) = \begin{cases} A_0(1-e^{-t/\tau_0}) & 0 < t < t_1 \\ A_0(e^{t_1/\tau_0}-1)e^{-t/\tau_0} & t_1 < t < t_2 \end{cases} \quad (1)$$

Here $t_1 = 22s$ and $t_2 = 44s$ for tape cycle settings in ^{162}Gd. The measured results are shown in Fig. 7 and Table III. The 205 and 330 gates should give the halflife of the possible high spin state of ^{162}Eu. The 165 and 253 keV gates were also used to compare to the result in Ref. [13]. These results do not show a clear difference in the halflives. From the intensity measurement in Table II, direct β feeding contributes ~70 % of the 863-keV level γ ray (791 and 863) intensities. Only the 863-keV gate was used in the current work, because the 791-keV is strongly contaminated by the 793- keV transition (more than half of the peak in Fig. 2) in ^{81}As. The result for the 863 gated halflife is consistent with the other gates discussed above. The 856 keV transition is contaminated by the 857 keV transition in ^{126}Te. The measured value of 10.8(5) s for 72 keV transition shows some difference from the other gates used in the present work. Such difference may be due to contamination of the 73 keV $K_{\alpha 2}$ of Pb. The 43 keV K_α x-ray of the Gd gate is also used for comparision. The Tb element also has a 44 keV K_α, but the contribution can be neglected, for the reason discussed below. The strong 403, 442 keV transitions in ^{162}Tb reported in Ref. [19] are ~ 4.5% and 5.3% of the 165 keV transitions in ^{162}Gd in the total γ ray spectrum in Fig. 2, respectively. These ^{162}Tb transitions are weak in the spectrum and do not generate significant internal conversion with x-rays. In all, the result from the present work does not show evidence for two different halflives in ^{162}Eu. It is possible that the reported [13] 160.2(24) keV isomer in ^{162}Eu only decays to the ground state of ^{162}Eu, or the halflives of the two state in ^{162}Eu are very close. The possible 160 keV isomeric transition in ^{162}Eu is not seen in our data. The data do show some very weak evidence for a 103-57 keV coincidence and a 99-61 keV coincidence. However, they are not considered as the cascades linking the 160 keV isomer and the ground state in ^{162}Eu because of the lack of confirmation in previous ^{162}Sm β decay to ^{162}Eu data.

TABLE III. Table of the halflives of ^{162}Eu by gating on different γ rays. The results are compared with previous experimental data.

Reference	Gates	Eu Halflife (s)	Depopulating Spin
[17]	K x-ray	10.6(10)	
[26]	ion-β	11.8(14)	
[13]	165,254	15.0(5)	4^+,6^+
this work	205,330	12.3(6)	(6^-)
	165	12.0(2)	4^+
	254	11.6(4)	6^+
	863	11.7(12)	2^+
	72[a]	10.8(5)	2^+
	43 (K_α)	11.6(3)	

a: this gate is contaminated.

B. ^{164}Gd

A newly developed level scheme for ^{164}Gd is shown in Fig. 8 with 16 new transitions, 13 new levels, and 2 transitions that were previously observed [16] now, for the first time, placed into the level scheme. Table IV denotes the list of the γ ray energies, intensities, initial and

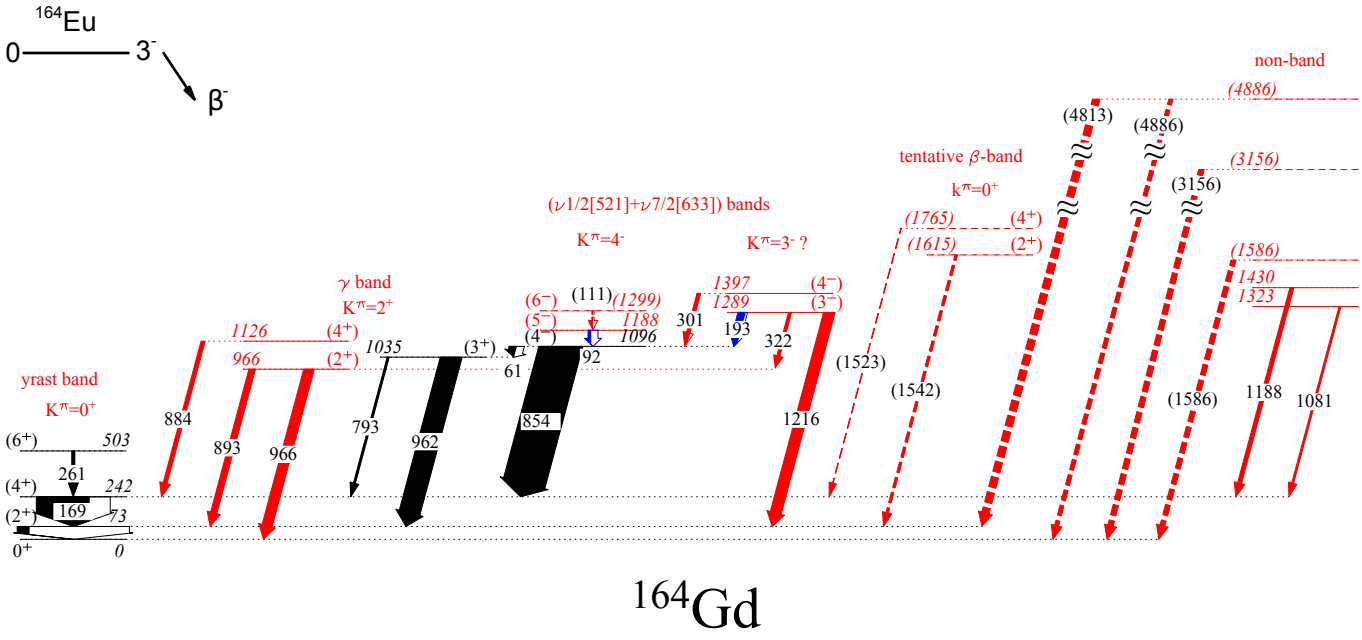

FIG. 8. The level scheme of ^{164}Gd as seen by the β-decay of ^{164}Eu. Red levels and transitions are newly observed in this work. Blue transitions are previously observed [16], but had not been placed in the level scheme. Other previously reported transitions are labeled in black.

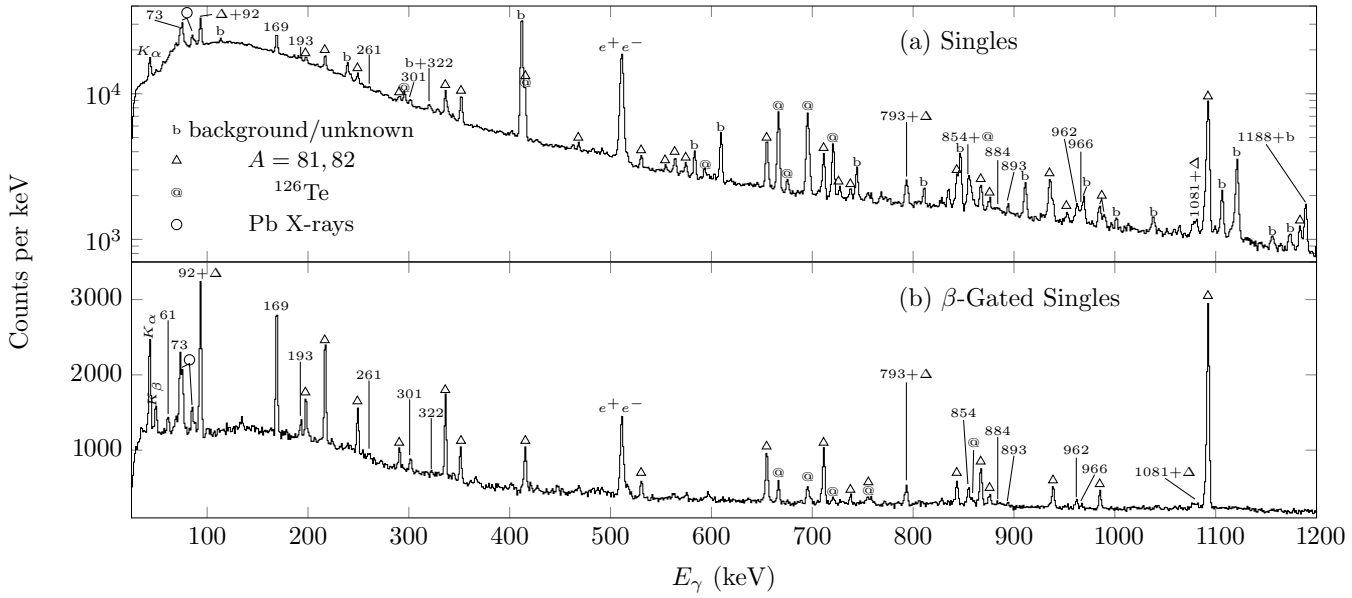

FIG. 9. Spectra from the LeRIBSS ^{164}Eu β-decay data for (a) γ ray singles, (b) β-gated γ ray singles.

final levels, and tentative spin-parity assignments. The ^{164}Eu parent nucleus is weaker populated in the beam than ^{162}Eu which results in a slightly different data analysis process.

First, the ^{164}Gd data were compiled using a 1 μs coincidence window, which is the same coincidence time as the prompt event matrix in ^{162}Gd. Figure 9 shows the γ ray singles and β-gated γ ray singles. First the singles spectrum is generated by every γ ray interaction with any of the 16 HPGe crystals in the 4 clovers of the LeRIBSS station with no coincidence of any kind required. In this single spectrum, all but the weakest peaks from ^{164}Gd can be seen, as well as the greatest number of contamination peaks. The way of generating this spectrum is the same as the one in Fig. 2 in ^{162}Gd. Second, the β-gated singles are just like the singles except that any γ ray recoreded in the spectrum must be in coincidence with a β-ray. This drastically reduces the contaminant

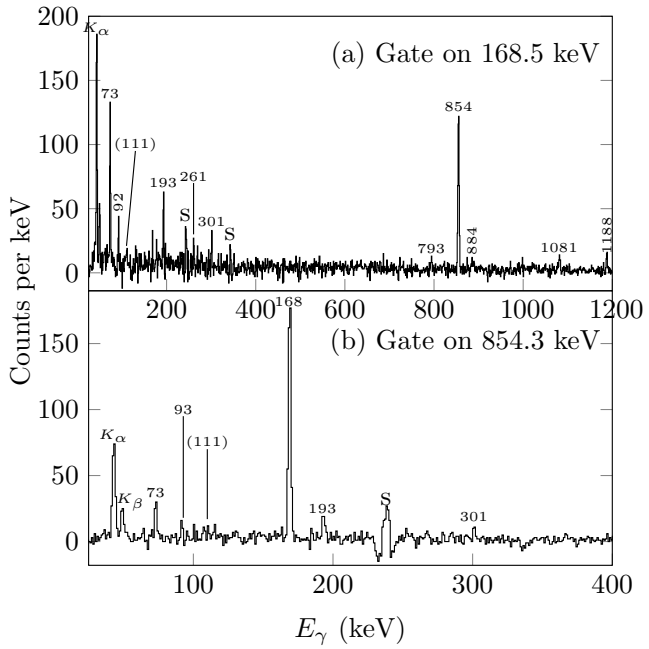

FIG. 10. Spectra from the LeRIBSS ^{164}Eu β-decay data for (a) a background subtracted gate on the 168.5 keV γ ray, (b) a background subtracted gate on the 854.3 keV γ ray.

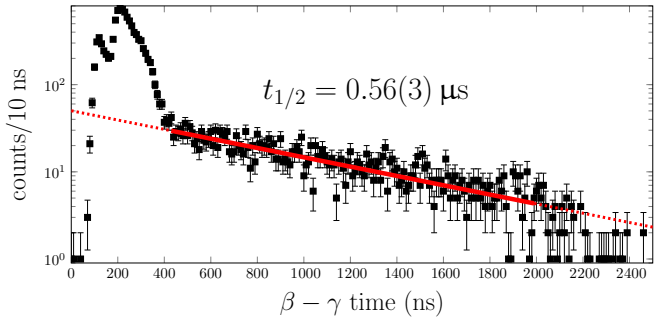

FIG. 11. (Color online) A plot of sum of gates on the 854.3 keV and 168.5 keV γ ray energies as a function of the $\beta - \gamma$ time. The data were recompiled using a 2 μs rolling coincidence window for the lifetime measurement. The fit shown between the end of the "bump" at ∼400 ns and 2 μs is used to determine the lifetime of the 1095.7 (4^-) isomer in ^{164}Gd.

peaks, as shown in the ^{162}Gd part before, and enhances the peak to background ratio of many of the peaks in which we are interested.

The spectra in Fig. 10 are both from background subtracted gates on γ rays, with no requirement of β-coincidence. Both of these coincidence spectra use add-back, where any gamma ray interactions in different crystals of the same clover are added back together under the assumption that they were in fact the same original γ ray. The background subtraction in these gates was done by subtracting gates on channels immediately to the left and right of the desired gate energies from the desired channels. Part (a) is a spectrum gated on

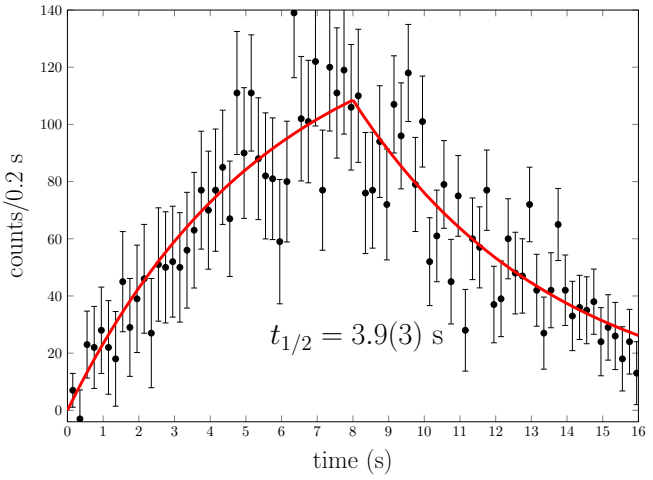

FIG. 12. (Color online)A plot of the measurement of the β-decay half-life of ^{164}Eu. Requiring β-coincidence, background subtracted γ ray gates on 72.9, 168.5, and 854.3 keV were summed to produce the time spectrum below. The grow-in and decay-out were fit simultaneously to produce the curves shown. The resulting half-life is 3.9(3) s.

the 169 keV transition in the ground state band, showing the clear 73, 92, 193, 793, 854 keV known transitions and new 261, 301 and 1081 keV transitions. Part (b) is a spectrum gated on the 854- keV transition, in which the 93, 193 and 301- keV transitions feeding the isomer can be clearly seen. The add-back background subtracted gate does not remove Compton scatter events, when a higher energy γ ray Compton scatters into a different clover detector. These scatter events create diagonal lines in the 2-D histogram from which these gates were taken, meaning that the background gates see the scatter peak at higher or lower energy than the gate energies and create sharp negative peaks in the final spectrum on either side of the cross talk peak, making them easier to spot. Scatter peaks are labled with an S in Fig. 9.

The most prominent contaminants in our data are from the $A = 82$ and 81 chains. Transitions from these nuclei have been marked with triangles in Fig. 9. We end up with $A = 81$ nuclei in our data from $\beta - n$ decay. Further details on the γ rays produced by these $A = 81, 82$ contaminants can be found in references [28–33].

A number of contaminant γ rays exhibit one distinguishing feature in common; that they experience no coincidence with other γ rays or β-particles. These contamination γ rays can be confirmed by comparing the spectra from ^{162}Gd in Fig. 2 and ^{164}Gd. These have been marked with a letter b in Fig. 9. These coincidence-less peaks also show no time variation behavior, meaning that they cannot be contained in our beam or dependent on our tape cycle. One contaminant which can be identified is ^{126}Te (stable residue and Coulomb excited), due to its obvious coincidence relationships and well known energy structure [34, 35]. The transitions from ^{126}Te are marked by an "@" symbol in Fig. 9. Additionally, the

TABLE IV. Table of levels and γ rays in ^{164}Gd. Square brackets indicate that a value is tentative. Subscripts on spin-parity labels indicate band. Here E_i is the level energy populating the γ rays and E_f is the level populating the γ rays.

E_γ	I_γ	ΠL	E_i	J_i^π	E_f	J_f^π
61.0†	13(3)	E1	1095.7[a]	$[4_4^-]$	1034.7	$[3_\gamma^+]$
72.9	23(6)	[E2]	72.9[b]	$[2_g^+]$	0.0[c]	0_g^+
91.6†	5(2)	[M1]	1187.3	$[5_4^-]$	1095.7[a]	$[4_4^-]$
[110.7]∗	1.6(13)	[M1]	[1298.0]	$[6_4^-]$	1187.3	$[5_4^-]$
168.5	100(6)	[E2]	241.4	$[4_g^+]$	72.9[b]	$[2_g^+]$
192.8†	13(2)	[M1]	1288.5	$[3_3^-]$	1095.7[a]	$[4_4^-]$
260.7	5.3(9)	[E2]	502.1	$[6_g^+]$	241.4	$[4_g^+]$
300.8∗	11(4)	[M1]	1396.5	$[4_3^-]$	1095.7[a]	$[4_4^-]$
322.2∗	8(4)	[E1]	1288.5	$[3_3^-]$	966.3	$[2_\gamma^+]$
793.3	3.7(15)		1034.7	$[3_\gamma^+]$	241.4	$[4_g^+]$
854.3	81(7)		1095.7[a]	$[4_4^-]$	241.4	$[4_g^+]$
883.9∗	8(2)		1125.3	$[4_\gamma^+]$	241.4	$[4_g^+]$
893.4∗	12(2)		966.3	$[2_\gamma^+]$	72.9[b]	$[2_g^+]$
961.8	40(4)		1034.7	$[3_\gamma^+]$	72.9[b]	$[2_g^+]$
966.3∗	19(6)		966.3	$[2_\gamma^+]$	0.0[c]	0_g^+
1080.8∗	3.5(14)		1322.2		241.4	$[4_g^+]$
1187.8∗	7(2)		1429.2		241.4	$[4_g^+]$
1215.6∗	21(3)		1288.5	$[3_3^-]$	72.9[b]	$[2_g^+]$
[1523.5]∗	< 5		[1764.9]	$[4_\beta^+]$	241.4	$[4_g^+]$
[1542.5]∗	< 17		[1615.4]	$[2_\beta^+]$	72.9[b]	$[2_g^+]$
[1585.7]∗	9(6)		[1585.7]		0.0[c]	0_g^+
[3156.3]∗	10(4)		[3156.3]		0.0[c]	0_g^+
[3789.8]∗∗	<10					0_g^+
[4812.6]∗	14(6)		[4885.5]		72.9[b]	$[2_g^+]$
[4885.5]∗	8(4)		[4885.5]		0.0[c]	0_g^+

[a] Isomeric state: $t_{1/2} = 0.56(3)$ μs, see figure 11.
[b] 2^+ state half-life: $t_{1/2} = 2.77(14)$ ns [36].
[c] Ground state half-life: $T_{1/2} = 45(3)$ s [37].
† Reported in [16] but not placed in the level scheme.
∗ Newly observed transitions in this work.
∗∗ Not placed in the level scheme.

Pb x-rays are from the activated Pb bricks used to shield the LeRIBSS station. The X-rays of Pb are marked by circles in Fig. 9.

The intensities displayed in Table IV were measured using both the total γ ray spectrum and the gated γ ray coincidence spectra, as shown in Figs. 9 and 10. The first spectrum is the γ ray singles spectra, which displays all γ rays detected during the nearly two hours of data collection, with no coincidence requirement or attempt to correct for losses due to effects like internal conversion. The second spectrum used was the β-gated singles, which is the same as the singles spectrum but has the added restriction that any γ ray included must be in coincidence with at least one electron, which reduces several sources of background contamination. The third and fourth spectra were background-subtracted gates on the 168.5 and 854.3- keV γ rays, respectively. Both the singles, and β-gated singles were normalized such that the intensity of the 168.5- keV γ ray was 100. The gate on 168.5 keV was normalized so that the 854.3 keV γ ray was equivalent to what was measured in the singles spectrum. The 854.3 keV gate was normalized by the intensity of the 192.8 keV γ ray, compared to its weighted average intensity in both the singles and β-gated singles spectra. In the single total spectra some transitions were contaminated by the mass 81, 82 transitions or too weak to measure, and hence the γ-ray gated spectra were used to obtain the energies and intensities. However, transitions populating the 1095 keV isomer would be attenuated when gating on transitions below it and result in some uncertainty.

The internal conversion coefficient of the 61.0 keV transition was measured by comparing the 61.0-, 793.3- and 961.8- keV γ ray intensities in the 192.8- keV transition gate above the isomer. The sum of the gated intensities of the two transitions depopulating the 1034.7 keV state fed by the 61.0 keV transition are taken as the total gated intensity $(\gamma + e^-)$ of the 61.0 keV transition. This gated intensity is compared to the measured gated intensity of the 61.0 keV γ ray transition. This means that the internal conversion coefficient of this 61.0 keV transition is

$$\alpha_{61} = \frac{I_{961} + I_{793}}{I_{61}} - 1 \qquad (2)$$

where α is the internal conversion coefficient and I is the measured γ ray intensity of a transition. The one complication to this is that, in the 192.8 keV gate, the 793.3 keV transition is barely identifiable above background, and thus too week to fit. The branching ratios of the 793.3 and 961.8 keV transitions from the total γ ray intensities in Table IV were used to determine the intensity of the 793.3 keV transition. These measured intensities of the 962 and 61 keV transitions and the calculated intensity of the 793 keV transition in this background subtracted 192.8 keV gate are used to deduce the internal conversion coefficient of the 61 keV transition. The experimentally measured internal conversion coefficient for this transition is 1.0(7). By comparing to the theoretical value for 1.1 E1, 8.4 M1 and 17 E2 in Ref. [38], the 61 keV transition is determinted to be an E1 transition by brIcc [38].

The lifetime of the 1095.7 keV state has been measured to be 0.56(3) μs. This measurement was conducted by measuring the exponential decay rate from the $\beta-\gamma$ time, or the time between the detection of an electron and the detection of a γ ray, by using a 2 μs rolling coincidence for longer observation of the isomer. In the $\beta-\gamma$ time vs. γ ray energy plot, the sum of the 854.3 and 168.5 keV γ rays was used for this measurement. The resulting summed gate is displayed in Fig. 11. In Fig. 11, first is the large sudden rise and rapid drop caused by fundamental limitations of our detector crystals. The second feature is caused by the decay of the isomer. An exponential decay

fit was performed, which appeared as a straight line on a logarithmic graph, as seen in Fig. 11. This section of the graph has been fit to determine the lifetime of the 1095.7 keV state. The third segment of Fig. 11 is the appearance of a shorter lifetime starting at 2 μs. This effect is caused by the nature of the "rolling" coincidence by which our data were compiled. This section was not included in the fit to determine the lifetime of the 1095.7 keV state.

Finally, the lifetime of the ^{164}Eu β-decay parent of ^{164}Gd has been measured by examining the tape cycles, as shown in Fig. 12. A 2-d histogram was generated which gives γ ray energy vs. time within a tape cycle, and consists in the sum of all tape cycles. As noted in the experimental setup section, the tape cycle was 8 s beam-on, followed by 8 s beam-off, for a total of 16 s. This means that our total tape cycle is only about 4 half-lives (previous: 4.2(2) s [16] and 3.80(56) s [26], see also [37]), with only two half-lives being allowed for each grow-in and decay-out, which increases the uncertainty in this lifetime measurement. While only 2 half-lives is shorter than desired for the measurement of the ^{164}Eu half life, it does minimize some the presence of contaminants from our beam. For example, it mostly precludes population of ^{164}Tb from the β-decay of ^{164}Gd, as that half life is 45(3) s [39]. Background subtracted gates on 72.9, 168.5, and 854.3- keV transitions were combined for more statistics. Both the grow-in and decay out were fit simultaneously with a piecewise function as also stated in Eq. (1) in Ref. [22]. From this fit we deduced the half life of ^{164}Eu to be 3.9(3) s, in agreement with the 4.15(20) s NNDC accepted half life [37]. The result of these gates and fitting is shown in Fig. 12.

IV. DISCUSSION

A. J^π assignments of ^{162,164}Eu

The β-feeding of levels in ^{162}Gd can be deduced from the γ ray decay in and out intensity balance. The calculated values for strongly populated levels are 72 keV 2^+, 65(30); 236 keV 4^+, 9(8); 490 keV 6^+, 16(3); 863 keV 2^+, 31(4); 927 keV 3^+, 26(3); 1448 keV 6^-, 21(3). The accurate percentage of β-feeding cannot be obtained because of the possibility for two different ^{162}Eu branches. The ground state β-feeding can be calculated from the ^{162}Gd and the daughter ^{162}Tb counts ratio. From Eq. 1, the number of the created ^{162}Gd atoms is:

$$N(^{162}\mathrm{Gd}) = \int_{t_1}^{t_2} I_0(t)dt \qquad (3)$$

Here taking $T_{1/2} = 11.8s$, which is the weighted average of the measurements of gating on 43, 165, 254, 205+330, 863 keV transitions by neglecting the possible difference between the β-decay halflives of the ^{162}Eu ground state and 160- keV isomer, one obtains $\tau_0 = T_{1/2}/ln(2) = 17.0s$ and $N(^{162}\mathrm{Gd}) = 18.616A_0$ (A_0 is defined in Eq. (1)). Similar to the Eq. in Ref. [22], the total number of ^{162}Gd atoms left during the tape cycle without decay is the integral:

$$N(^{162}\mathrm{Gd})_R = \int_0^{t_2} e^{-(t_2-t)/\tau'} I_0(t)dt \qquad (4)$$

Taking a weighted average from Refs. [18, 19], $T_{1/2}(^{162}\mathrm{Gd}) = 503s$, one can get $\tau' = T_{1/2}(^{162}\mathrm{Gd})/ln(2) = 725s$. The integral is $N(^{162}\mathrm{Gd})_R = 18.062A_0$. The number of ^{162}Tb atoms created from decay is the difference of these two $N(^{162}\mathrm{Tb}) = N(^{162}\mathrm{Gd}) - N(^{162}\mathrm{Gd})_R = 0.554A_0$. Thus, $N(^{162}\mathrm{Gd})/N(^{162}\mathrm{Tb}) = 33.6$. The $N(^{162}\mathrm{Tb})$ can be evaluated by adding the 403 and 442 keV transition intensities depopulating the 442 keV level, which has 95.5% β-feeding according to Ref. [19]. This value times the 33.6 factor can give the $N(^{162}\mathrm{Gd})$ value. The $N(^{162}\mathrm{Gd})$ contains 72, 863 keV ground state γ rays and ground state β-feeding. By doing the subtraction, the ^{162}Gd ground state β feeding is 34(39) (not percentage). This value would be an upper limit for possible ^{162}Gd in the beam. In order to explain the relatively strong β-feeding of the 2^+, 3^+, 4^+, 6^+, 6^- ^{162}Gd states, we propose the ^{162}Eu ground state and 160 keV isomer to be 6^+ $\pi 5/2[413] \otimes \nu 7/2[633]$ and 3^- $\pi 5/2[413] \otimes \nu 1/2[521]$, respectively, by comparing with the neighboring nuclei $N = 99$ $\nu 7/2[633]$ ground state for ^{161}Sm [11, 40], ^{163}Gd [41], ^{165}Dy [42]; $Z = 63$ $\pi 5/2[413]$ ground state for ^{159}Eu [43]; and $N = 99$ $\nu 1/2[521]$ isomer in ^{163}Gd [41, 44] 138 keV 23.5(10)s, ^{165}Dy 108 keV 1.257(6)min [42].

From the intensity data shown in Table IV, we can calculate the combined β- and γ-feeding for each level in ^{164}Gd. The results of this analysis are shown in Table V. Since the known Q-value for the β-decay of ^{164}Eu is 6.39(5) MeV [45], it seems likely that other weak high energy states and γ rays are produced in the β-decay of ^{164}Eu which remain unobservable in our data due to the low efficiencies of the HPGe detectors at higher energies. Thus, the current β-feeding measurements and the determined $\log(ft)$ values for ^{164}Gd are only valid and referable for strong β-feeding levels. However, we can still attempt to deduce the spin and parity of the ground state and β-decaying isomers of ^{164}Eu. Since the relatively reliable spins of 241- keV 4^+, 966- keV (2^+), 1035- keV (3^+), 1096- keV (4^-) states receive strong feeding, $3^\pm$ and 4^- are preferred for the ground state of ^{164}Eu. The logft value for the 1095.7 (4^-) state lies on the edge of an allowed transition. Thus, 3^- and 4^- are more favored. The 1187 keV (5^-) level also receives strong β-feeding, but the value is not very reliable due to the strong contamination of the 93 keV transition from ^{81}As. The proton and neutron Nilsson orbitals near the fermi energy are $\pi 5/2^+[413]$, $\pi 5/2^-[532]$, $\pi 3/2^+[411]$, $\nu 1/2^+[521]$, $\nu 7/2^+[633]$. The only combination is $3^-\pi 5/2[413] \otimes \nu 1/2[521]$. This assignment is consistent with the tentative assignment from nuclear data sheets (Ref. [37]).

TABLE V. The γ ray feeding, outflow and β-feeding of excited levels in ^{164}Gd from the β-decay of ^{164}Eu calculated from Table. IV. Ground state β-feeding is assumed to be 0. Note the weakly populated levels are not accurate because of the possible unobserved high energy transitions due to low yield of population and low efficiency. Subscripts on spin-parity labels indicate their band, either a simple identifier for collective bands or the value of K for the quasi-particle bands.

$E_{\rm level}$ (keV)	I^π	γ-feeding	γ-outflow	Iβ	Iβ (%)	log(ft)
0.0	0_g^+	261(57)	0	$\sim$0	$\sim$0	
72.9	$[2_g^+]$	232(16)	214(61)	$<$46	$<$18	$>$6.3
241.4	$[4_g^+]$	108(8)	140(8)	31(11)	12(4)	6.4(2)
502.1	$[6_g^+]$	0	5.8(10)	5.8(10)	2.2(4)	7.1(1)
966.3	$[2_\gamma^+]$	8(4)	31(6)	24(7)	9.2(27)	6.3(2)
1034.7	$[3_\gamma^+]$	28(7)	43(4)	16(13)	6.1(50)	6.5(4)
1095.7	$[4_4^-]$	47(8)	108(14)	61(16)	23(6)	5.9(2)
1125.3	$[4_\gamma^+]$	0	8(2)	8(2)	3.1(8)	6.8(1)
1187.3	$[5_4^-]$	4(3)	18(6)	14(7)	5.4(27)	6.5 (3)
1288.5	$[3_3^-]$	0	47(6)	47(6)	18(2)	5.9(1)
[1298.0]	$[6_4^-]$	0	4(3)	4(3)	1.5(11)	7.0(4)
1322.2		0	3.5(14)	3.5(14)	1.3(5)	7.0(2)
1396.5	$[4_3^-]$	0	12(4)	12(4)	4.6(15)	6.5(2)
1429.2		0	7(2)	7(2)	2.7(8)	6.7(2)
[1585.7]		0	9(6)	9(6)	3.4(23)	6.5(4)
[1615.4]	$[2_\beta^+]$	0	<17	<17	$<$6.5	$>$6.2
[1764.9]	$[4_\beta^+]$	0	<5	<5	$<$2	$>$6.7
[3156.3]		0	10(4)	10(4)	3.8(15)	5.7(2)
[4885.5]		0	22(7)	22(7)	8.4(27)	4.1(2)

B. High K quasiparticle states and hindrance

According to Patel *et. al.*,[11] and Yokoyama *et. al.*,[9] (same research group), the decay of the 1095.7- keV level in ^{164}Gd is hindered by a large change in K. For the 854 keV γ ray, $\Delta K = -4$, even though $\Delta J = 0$. An experimental hindrance factor can be defined as $f_\nu \equiv \left(t^\gamma_{1/2}/t^W_{1/2}\right)^{1/\nu}$, where $t^W_{1/2}$ is the Weisskopf predicted half life for the transition, $t^\gamma_{1/2}$ is the γ ray partial half life, $\nu = |\Delta K| - L$, and L is the multipole order of the transition (i.e. EL or ML). Patel *et. al.* [11] reports $f_3 = 1.4 \times 10^3$ for the 854 keV γ ray, while Yokoyama *et. al.*, [9] quotes $f_3 = 1.28(3) \times 10^3$. The difference between these two results primarily stems from differing branching ratios of the 61 keV transition compared to the 855 keV γ ray. The present experiment has better statistics than either Patel *et. al.*, or Yokoyama *et. al.*, and a new half life measurement which is consistent with both of their half life measurements. Based on these considerations we have found $f_3 = 1.27(7) \times 10^3$ for the 854 keV transition and $f_1 = 4.5(13) \times 10^6$ for the 61 keV transition. The current independent measurement confirms the measurements of Yokoyama *et. al.* with $f_3 = 1.28(3) \times 10^3$. These two hindrance factors were measured with partial half lives $t^\gamma_{1/2}(61) = 4.5(13)\,\mu$s, $t^{IC}_{1/2}(61) = 4.1(36)\,\mu$s, and $t^\gamma_{1/2}(854) = 0.75(12)\,\mu$s, derived from the branching ratios of the 854 and 61 keV γ rays and the ICC of the 61 keV transition. For ^{162}Gd, the hindrance factor of the 330 keV transition depopulating the 1449 keV (6^-) isomer can also be obtained for comparison. With $\Delta K = 4$, $\nu = 1$ and $t_{1/2} = 99(3)\mu s$, the calculated f_v is 2325(23). This value is not only larger than the ^{164}Gd 4^- value, but also significantly larger than the E1 transitions depopulating the 6^- $\nu 5/2[512] \otimes 7/2[633]$ isomer in ^{164}Sm f_v =487(38), ^{166}Gd f_v =356(7) reported in Ref. [12]. A 6^- $\nu 5/2[523] \otimes 7/2[633]$ $t_{1/2} = 339(20)$ns isomer was reported in ^{158}Nd [7]. The 1197 keV E1 transition (followed by 233 and 152 keV transitions) decaying from the ^{158}Nd isomer to the ground state band leads to a factor $f_v = 76(1)$. From the current calculation as discussed later, the 1449 keV 6^- isomer in ^{162}Gd is also proposed to be 6^- $\nu 5/2[523] \otimes 7/2[633]$. Such differences may indicate that the 152, 233, 1197- keV transitions reported in Ref. [7] in ^{158}Nd were wrongly placed – the correct order may be 152 keV $4_g^+ \rightarrow 2_g^+$, 1197 keV $5_\gamma^+ \rightarrow 4_g^+$ and 233 keV $6^- \rightarrow 5_\gamma^+$. Such an assignment gives f_v =264(5) and is generally close to the values in ^{164}Sm and ^{166}Gd.

By using the intensity data in Table IV, the $B(\Pi L)$ ratios can be determined for the transitions out of the 966.3, 1034.7 and 1095.7, and 1288.5- keV levels in ^{164}Gd. All of the measured ratios are presented in Table VI.

The assignement about the 1288.5 keV level in ^{164}Gd can be made based on the $B(\Pi 1)$ ratios and final spin-parity of its three depopulating γ rays. First, it decays to the 72.9- keV 2_g^+, 966.3- keV (2_γ^+), and 1095.7- keV (4_4^-) states, thus its own spin and parity must be 2^-, $3^\pm$, or 4^+, because only $M1$, $E1$, and $E2$ transitions are commonly observed. Second, the reduced transition probabilities of the 192.8 and 322.1 keV transitions are clearly much higher than that of the 1215.6 keV transition in Table VI, which favors a high K for the 1288.5- keV level. By comparing with the reduced transition probability ratios found in Lesher *et. al.*,[46] for ^{160}Gd, nearly all collective states can be rule out. In Lesher *et. al.*, the levels of the γ-vibrational band of ^{160}Gd decay only to the ground state band, while the 1288.4 keV state in ^{164}Gd is observed decaying to both γ-vibrational and ground state bands. Furthermore, the energy space for

TABLE VI. Reduced transition probability ratios measured for ^{164}Gd as seen by the β-decay of ^{164}Eu. Subscripts on spin-parity labels indicate band, either a simple identifier for collective bands or the value of K for the quasi-particle bands.

γ ray Decay Pattern	Ratio
$B(E2; 966; 2_\gamma^+ \rightarrow 0_g^+)/B(E2; 894; 2_\gamma^+ \rightarrow 2_g^+)$	1.1(3)
$B(E2; 962; 3_\gamma^+ \rightarrow 2_g^+)/B(E2; 793; 3_\gamma^+ \rightarrow 4_g^+)$	4.1(17)
$B(E1; 854; 4_4^- \rightarrow 4_g^+)/B(E1; 61; 4_4^- \rightarrow 3_\gamma^+)$	0.0027(7)
$B(E1; 1216; 3_3^- \rightarrow 2_g^+)/B(E1; 322; 3_3^- \rightarrow 2_\gamma^+)$	0.05(3)
$B(E1; 1216; 3_3^- \rightarrow 2_g^+)/B(M1; 193; 3_3^- \rightarrow 4_4^-)$	0.0063(13)
$B(E1; 322; 3_3^- \rightarrow 4_4^-)/B(M1; 193; 3_3^- \rightarrow 4_4^-)$	0.12(7)

the 1288.5- keV state does not match for it to be a γ-vibrational state. One can also rule out $K^\pi = 0^-, 1^-$ octupole vibrational bands, as they are also observed to only decay to the ground state band in ^{160}Gd by Lesher *et. al.*, The most likely option by observing Lesher *et. al.*, is the 3^- of a 2^- octupole vibrational band. Lesher *et. al.*, observes this state in ^{160}Gd decaying to the 4^+_γ, 3^+_γ, and 2^+_γ with about equal intensities and the 4^+_g with about 0.7% the reduced transition probability of the other transitions from this level. We rule this level out for ^{164}Gd, because we observe it decaying only to the 2^+_γ instead of all three γ-vibrational states, and observe decay to the 2^+_g state, rather than the 4^+_g state. The 1288.5- keV level cannot be the 4^+_β level, as decay from this state to the γ-vibrational band would be forbidden, as it simultaneously would create a γ-phonon while destroying a β-phonon. This statement assumes no $\beta - \gamma$ mixing (i.e. $Z_{\beta\gamma} = 0$), and may not be true. However, comparison with the β-band of ^{160}Gd cited in Lesher *et. al.*, indicates that the assumption of no decay from the β-band to the γ-band holds true for neutron-rich, even-even Gd isotopes. Thus, the 1288.5- keV level is most likely to be a quasi-particle state. According to its almost allowed logft value, 2^-, 3^- and 4^- are the most propable candidates. Combining with the decay pattern discussed above, we believe that the 1288.5- keV level is likely a 3^- $\nu 1/2[521] \oplus \nu 7/2[633]$ state, and favors decay to the 1095.7, (4^-) level due to the shared configuration. The assignment of this configuration is in consistent with the 1094 keV 4^- $\nu 1/2[521] \oplus \nu 7/2[633]$ isomeric state reported in ^{168}Er [48]. Further details will be discussed in the calculation part.

The 4886- keV level in ^{164}Gd has a very small logft value for an allowed transition. This value favors 2^-, 3^- or 4^- for its spin/parity assignment. If the spin/parity is 2^-, it could be some other quasiparticle or collective bandhead. If the spin/parity is 3^-, a strong 4886 keV E3 transition would indicate strong octupole deformation or correlation. However, since the ownership of this transition is not very certain, this judgement is not very clear.

C. γ band structure

Since the ^{160}Gd(t,p)^{162}Gd reaction [15] provided spin/parity assignments of the γ-band and β-band levels, the ^{162}Gd data obtained in the current work, together with neighboring Gd isotopes, can help investigate the γ-band structure/assignments in ^{164}Gd. From Alaga rules [47], the ratio of $B(EL)$ values for transitions out of the same state is the ratio of the square of Clebsch Gordon coeficients

$$\frac{B(EL: J_i \to J_f)}{B(EL: J_i \to J'_f)} = \frac{\langle J_i K_i L \Delta K | J_f K_f \rangle^2}{\langle J_i K_i L \Delta K' | J'_f K'_f \rangle^2} \qquad (5)$$

This equation gives $B(E2; 2^+_\gamma \to 0^+_g)/B(E2; 2^+_\gamma \to 2^+_g)$=0.7, $B(E2; 2^+_\gamma \to 2^+_g)/B(E2; 2^+_\gamma \to 4^+_g)$=20, $B(E2; 3^+_\gamma \to 2^+_g)/B(E2; 3^+_\gamma \to 4^+_g)$=2.5 and $B(E2; 4^+_\gamma \to 2^+_g)/B(E2; 4^+_\gamma \to 4^+_g)$=0.34. The $B(E2)$ ratios of transitions from the 966.3- keV, (2^+_γ) and 1034.7- keV, (3^+_γ) states shown in Table VI are in agreement with the Alaga rules ratio and confirm the γ-band assignment of these levels. The 4^+ level of the γ-band only has one transition decaying to the 4^+ ground state. However, the Alaga rules predict the 4^+_γ to 2^+_g weaker than this 4^+_γ to 4^+_g. Detailed γ band levels, 2γ band levels, as well as other quasiparticle bands are discussed in the following section.

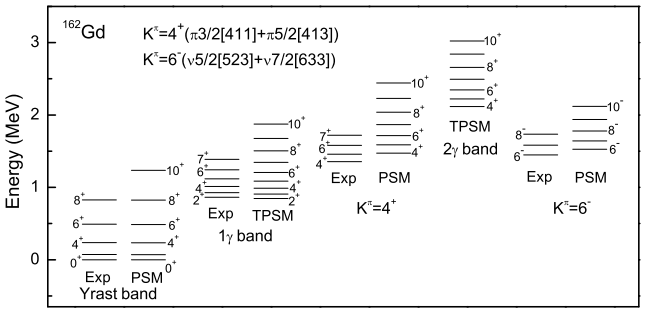

FIG. 13. Projected shell model calculations for the band structures in ^{162}Gd, compared with the experimental data.

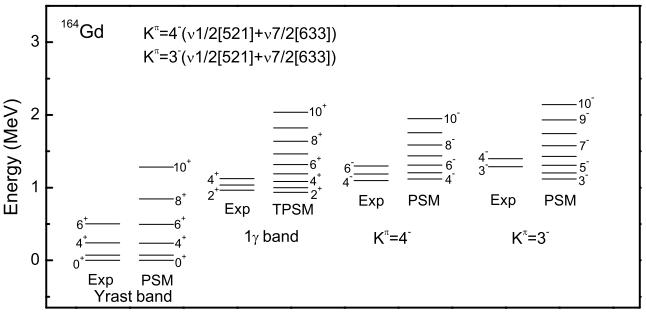

FIG. 14. Projected shell model calculations for the band structures in ^{164}Gd, compared with the experimental data.

D. Projected Shell Model and Triaxial Projected Shell Model Calculation

Projected shell model (PSM) [49–54] and Triaxial projected shell model (TPSM) calculations [55, 56] have been performed for comparison with the level schemes of the g.s. bands, isomer states and γ-vibrational bands in ^{162,164}Gd. In the present calculations, the Nilsson energy levels are calculated with deformation parameters ϵ_2=0.275, ϵ_4=0.007, ϵ'=0.115 for ^{162}Gd and ϵ_2=0.275, ϵ_4=0.000, ϵ'=0.110 for ^{164}Gd taken from Möller *et al.*[57], respectively. The ϵ' is the the triaxial deformation parameter in the TPSM calculation. The monopole-pairing strength is taken to be $G_M = [G_1 \mp G_2(N-Z)/A]/A$, "-" for neutrons and "+" for protons, with $G_1 = 20.12$

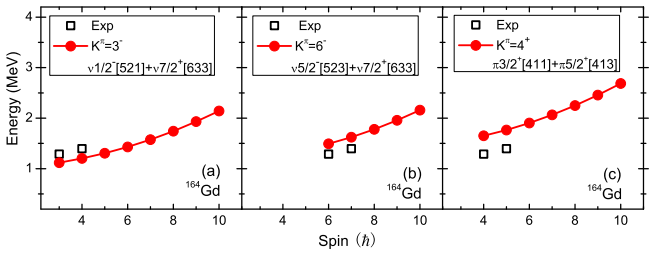

FIG. 15. The calculated energy levels of $K^\pi = 3^-$, $K^\pi = 6^-$ and $K^\pi = 4^+$ two quasiparticle bands and comparison with the experimental data.

and $G_2 = 13.13$ being the coupling constants. The quadrupole-pairing strength G_Q is assumed to be proportional to G_M, with the proportionality constant being fixed to be 0.16. These strengths are consistent with those used in previous works for the same mass region [52, 54].

From the calculation, the yrast band and 1γ band in ^{162,164}Gd have been well reproduced from the theory shown in Fig.13 and Fig.14. For ^{162}Gd, band (5) with a band-head at the 1354- keV level favors 4^+ from the decay pattern to the 1γ band (2) in Fig.13. The calculation predicts the 2γ band-head at 2.12 MeV and the 4^+ $\pi 3/2[411] \otimes \pi 5/2[413]$ bandhead at 1.47 MeV.Therefore, the 4^+ band in ^{162}Gd is unlikely to be a 2γ band. Recent β-decay study [58] assigned 1071 keV 4^+ as hexadecapole band head. The 4^+ hexadecapole band in ^{160}Gd [58] has strong linking transitions to the ground state band but not the 1γ band. This decay pattern in ^{160}Gd is different from the current 4^+ band in ^{162}Gd. Thus, band (5) is proposed to be the 4^+ $\pi 3/2[411] \otimes \pi 5/2[413]$ two proton quasiparticle band, instead of a 2γ-vibrational band. The calculations also predict the 6^- $\nu 5/2[523] \otimes \nu 7/2[633]$ at 1.53 MeV giving the same assignment with Ref. [13]. Note that in Fig.14 the 4^- $\nu 1/2[521] \otimes \nu 7/2[633]$ band has been very well reproduced by the PSM calculation. The configuration assignments of 6^- and 4^- isomer states in ^{162,164}Gd play an important role to discuss the location of the deformed shell gap which is discussed in Ref. [12, 13, 26]. Our coming theoretical work[54] will investigate the changes of deformed shell gap with the neutron numbers at $N \sim 100$ neutron-rich mass region. To discuss the configuration of the possible 3^- state with bandhead at 1289 keV in ^{164}Gd, PSM calculation is performed with the assumption of 3^-, 6^- and 4^+ bandhead at 1289 keV and compared with the theoretical energy levels in Fig.15. In the PSM calculation, the configurations of $K^\pi = 3^-$, $K^\pi = 6^-$ and $K^\pi = 4^+$ are assigned with $\nu 1/2[521] \otimes \nu 7/2[633]$, $\nu 5/2[523] \otimes \nu 7/2[633]$ and $\pi 3/2[411] \otimes \pi 5/2[413]$. The experimental data can be well reproduced by assuming the assignment of $K^\pi = 3^-$ and $K^\pi = 6^-$, however, from the transition point of view, $K^\pi = 3^-$ $\nu 1/2[521] \otimes \nu 7/2[633]$ and $K^\pi = 4^+$ $\pi 3/2[411] \otimes \pi 5/2[413]$ configurations are reasonable to explain the observed transition of 1216 keV. For further configuration assignments of a possible 3^- state, more experimental data are expected in the future experimental work.

V. CONCLUSION

In conclusion, the structures in ^{162,164}Gd have been studied from ^{162,164}Eu β-decay. New energy levels, γ rays and band structures have been reported. The halflife of the isomeric state in ^{162}Gd has been measured for the first time. The isomeric state in ^{164}Gd has been remeasured and is in agreement with the previous measurements. Projected shell model calculations have been performed and found to be in good agreement with the experimental data for the collective and quasiparticle band structures.

ACKNOWLEDGMENTS

We would like to acknowledge the Holifield Radioactive Ion Beam Facility and staff for their critical role in obtaining these data. Research at ORNL is supported by the Office of Nuclear Physics, U.S. Department of Energy, grant no. DE-AC05-00OR22725. The work at Vanderbilt University is supported by the US Department of Energy under Grant No. DE-FG05-88ER40407. The U.S. Department of Energy supported participants from Mississippi State University under grant NO. DE-SC00144448. Participants from the University of Tennessee were funded by the Office of Nuclear Physics, U.S. Department of Energy under Award No. DE-FG02-96ER40983 and the National Nuclear Security Administration under the Stewardship Science Academic Alliances program through DOE Award No. DE-NA0002132. The work at Huzhou University was supported by the National Natural Science Foundation of China under Grant No. U1832139, 11947410, and work at Shanghai Jiao Tong University was supported by the National Natural Science Foundation of China under Grant No. U1932206, and by the National Key Program for S&T Research and Development of China (No. 2016YFA0400501). We would also give special thank to professor Masato Asai at Japan Atomic Energy Agency Sector of Nuclear Science Research Advanced Science Research Center, professor M. Shibata at Nagoya University and professor Hayashi Hiroaki at Kanazawa University for private communications.

[1] H. Mach *et al.*, Phys. Rev. Lett. **56**, 1547 (1986).

[2] R. Surman, J. Engel, J. R. Bennett, and B. S. Meyer, Phys. Rev. Lett. **79**, 1809 (1997).

[3] E. F. Jones *et al.*, J. Phys. G: Nucl. Part. Phys. **30**, L43-L48 (2004).
[4] P.-A. Soderstrom *et al.*, Phys. Rev. C **81**, 034310 (2010), and the references therein.
[5] P. Moller, J. Nix, W. Myers, and W. Swiatecki, At. Data Nucl. Data Tables **59**, 185 (1995).
[6] G. S. Simpson *et al.*, Phys. Rev. C **80** 024304 (2009).
[7] E. Ideguchi *et al.*, Phys. Rev. C **94**, 064322 (2016).
[8] E. H. Wang *et al.*, Phys. Rev. C **90**, 067306 (2014).
[9] R. Yokoyama *et. al.*, Phys. Rev. C **95**, 034313 (2017).
[10] Z. Patel *et al.*, Phys. Lett. B **753**, 182-186 (2016).
[11] Z. Patel *et al.*, Phys. Rev. C **96**, 034305 (2017).
[12] Z. Patel *et al.*, Phys. Rev. Lett. **113**, 262502 (2014).
[13] D. J. Hartley *et al.*, Phys. Rev. Lett. **120**, 182502 (2018).
[14] L. Gaudefroy *et. al.*, Phys. Rev. C **97**, 064317 (2018).
[15] G. Lovhoiden *et al.*, Phys. Scr. **34**, 691 (1986).
[16] A. Osa, S. ichi Ichikawa, M. Matsuda, T. K. Sato, and S.-C. Jeong, Nucl. Instrum. Methods Phys. Res., Sect. B vol. **266**, no. 19, pp. 4394 - 4397, 2008.
[17] R. C. Greenwood, R. A. Anderl, J. D. Cole, and H. Willmes, Phys. Rev. C **35**, 1965(R) (1987).
[18] J. C. Chang, G. Schupp and R. R. Hurst, Nucl. Phys. A **142**, 634-640 (1970).
[19] R. J. Gehrke, R. C. Greenwood, J. D. Baker and D. H. Meikrantz, Radiochim. Acta 31, 1 (1982).
[20] R. C. Greenwood, M. A. Lee, R. A. Anderl, Radiochim. Acta 43, 129 (1988).
[21] J. A. Winger *et al.*, Phys. Rev. C **81**, 044303 (2010).
[22] M. F. Alshudifat *et al.*, Phys. Rev. C **93**, 044325 (2016).
[23] M. Asai *et al.*, proceedings of the 3rd International conference on fission and properties of neutron-rich nuclei, pp 227, eds. J.H.Hamilton, A.V.Ramayya, H.K. Carter.
[24] D. Rabenstein and H. Vonach, Z. Naturforsch. 26a, 458 (1971).
[25] B. Singh, Nucl. Data Sheets, vol. **105**, pp. 223 - 418, (2005).
[26] J. Wu *et al.*, Phys. Rev. Lett. **118**, 072701 (2017).
[27] S. Ichikawa *et al.*, Phys. Rev. C **71**, 067302 (2005).
[28] A. Etile *et al.*, Phys. Rev. C **91**, 064317, (2015).
[29] P. Hoff and B. Fogelberg, Nucl. Phys. A, vol. **368**, no. 2, pp. 210 - 236, (1981).
[30] K. Miernik *et al.*, Phys. Rev. C **90**, 034311, (2014).
[31] S. Padgett *et al.*, Phys. Rev. C **82**, 064314, (2010).
[32] C. M. Baglin, Nucl. Data Sheets, vol. **109**, no. 10, pp. 2257 - 2437, (2008).
[33] J. K. Tuli and E. Browne, Nucl. Data Sheets, vol. **157**, pp. 260 - 494, (2019).
[34] L.-C. He *et al.*, Chin. Phys. C, vol. **41**, 044003, (2017).
[35] J. Katakura and K. Kitao, Nucl. Data Sheets, vol. **97**, no. 3, pp. 765 - 926, (2002).
[36] D. Nagae *et al.*, AIP Conference Proceedings, vol. **1224**, no. 1, pp. 156-160, 2010.
[37] B. Singh and J. Chen, Nucl. Data Sheets, vol. **147**, pp. 1 - 381, (2018).
[38] T. Kibedi *et al.*, Nucl. Instrum. Methods Phys. Res., Sect. A vol. **589**, no. 2, pp. 202-229, (2008).
[39] R. A. Anderl and R. C. Greenwood, J Radioanal Nucl Chem, vol. **142**, pp. 203 - 213, (1990).
[40] C. W. Reich, Nucl. Data Sheets, vol. **112**, Issue 10, 2497-2713 (2011).
[41] C. J. Zachary *et al.*, in preparation.
[42] A.K. Jain, A. Ghosh and B. Singh, Nucl. Data Sheets, vol. **107** 1075 - 1346 (2006).
[43] C. W. Reich, Nucl. Data Sheets, vol. **113**, Issue 1, 157-363 (2012).
[44] H. Hayashi *et al.*, Nucl. Instrum. Meth. A. Volume **747**, 41-51 (2014).
[45] Meng Wang, G. Audi, F.G. Kondev, W.J. Huang, S. Naimi and Xing Xu, Chinese Phys. C 41 030003 (2017).
[46] S. R. Lesher *et al.*, Phys. Rev. C **95**, 064309, (2017).
[47] G. Alaga, Phys. Rev. **100**, 432 (1955).
[48] C. Y. Wu *et al.*, Phys. Rev. C **68**, 044305 (2003).
[49] K. Hara and Y. Sun, Int. J. Mod. Phys. E **4**, 637 (1995).
[50] Y. Sun, Phys. Scr. **91**, 043005 (2016).
[51] Y.X. Liu, Y. Sun, X.H. Zhou *et al.*, Nucl. Phys. A 858, 11 (2011).
[52] Y. C. Yang, Y. Sun, S. J. Zhu *et al.*, J. Phys. G: Nucl. Part. Phys 37, 085110 (2010).
[53] X.Y. Wu, S. K. Ghorui, L.-J. Wang *et al.*, Phys. Rev.C **95**, 064314 (2017).
[54] Y. X. Liu, C. J. Lv, Y. Sun and Filip G. Kondev, J. Phys. G: Nucl. Part. Phys., accepted.
[55] J. A. Sheikh and K. Hara, Phys. Rev. Lett. **82**, 3968 (1999).
[56] Y. Sun, K. Hara, J.A. Sheikh, J. Hirsch, V. Velazquez and M. Guidry, Phys. Rev. C **61** 064323 (2000).
[57] P. Möller, A. Sierk, T. Ichikawa et al., At. Data Nucl. Data Tables **109-110**, 1 (2016).
[58] D. J. Hartley et al., Phys. Rev. C **101**, 044301 (2020).